NISTIR 6330

A Study of a Water-to-Water Heat Pump Using Hydrocarbon and Hydrofluorocarbon Zeotropic Mixtures

W. Vance Payne, II
Piotr A. Domanski
Jaroslaw Muller

Building and Fire Research Laboratory
Gaithersburg, Maryland 20899

United States Department of Commerce
Technology Administration
National Institute of Standards and Technology

NISTIR 6330

A Study of a Water-to-Water Heat Pump Using Hydrocarbon and Hydrofluorocarbon Zeotropic Mixtures

W. Vance Payne, II
Piotr A. Domanski
Jaroslaw Muller

Building Environment Division
Building and Fire Research Laboratory

May 1999

TABLE OF CONTENTS

List of Tables

List of Figures

A Study of a Water-to-Water Heat Pump Using Hydrocarbon and Hydrofluorocarbon Zeotropic Mixtures

W. Vance Payne, Piotr A. Domanski , and Jaroslaw Muller*

Abstract

This investigation compared the performance of R22 to the performance of propane (R290) and zeotropic mixtures of HFC's and hydrocarbons in a water-to-water heat pump. Baseline testing began with R22 and proceeded to R290, R32/290, R32/152a, and R290/600a. The use of brazed plate heat exchangers arranged in counterflow for both heating and cooling allowed glide matching using the zeotropic refrigerant mixtures. The performance of the system was characterized by air-side capacity, air-side COP, compressor RPM, and refrigerant conditions. Testing showed that the R32/290 (50/50 by mass) mixture produced the highest cooling COP for a given capacity averaging 17 % higher than R22 at standard conditions. When compared to the simulated direct expansion R22 system, the R32/290 cooling COP averaged 11 % lower. Heating tests showed that propane (R290) COP averaged 3 % lower than R22 in the direct expansion simulation and 5 % higher than R22 in the water-to-water tests. R32/290 heating COP averaged 10 % lower than R22 in the simulated direct expansion configuration.

Keywords: Water-to-water heat pump, zeotropic mixtures, glide matching, flammable, COP

* Guest Researcher from Technical University of Cracow, Institute of Thermal Engineering and Air Protection, Cracow, Poland

1: Introduction

With the success of the Montreal Protocol effectively regulating the use of chlorine-containing refrigerants, the trapping of infrared radiation by anthropogenic gases and the resulting increase of the earth's temperature is being recognized as a potentially critical global environmental problem (Albritton, 1997). A heat pump or refrigeration system has a direct and indirect impact on the earth climate. The direct impact is related to the Global Warming Potential (GWP) of the refrigerant molecule when released to the atmosphere. The indirect impact is related to the emission of carbon dioxide by a fossil-fuel power plant producing electricity, and hence is affected by the system efficiency and the electricity generation mix. Constructing a leak proof system may mitigate the direct impact, and increasing the system efficiency may reduce the indirect impact. Both impacts are combined in the concept of Total Equivalent Warming Impact (TEWI) (Calm, 1993).

Concerns about global warming have caused a re-evaluation of hydrofluorocarbons (HFCs) and their mixtures because their GWPs are considered to be excessive in some countries. This unfavorable sentiment may affect the two most touted R22 replacements, R407C (R32/125/134a) and R410A (R32/125), whose non-flammable HFC components, R134a and R125, contribute the most to those mixture's GWP values.

Flammable refrigerants, including flammable HFCs, have short atmospheric life times and low GWPs. So far, flammables have received limited attention in studies for residential heat pump applications because of liability concerns for refrigerant piping passing through the inhabited space. The chance of acceptance of flammable refrigerants would improve if they remain outdoors. The water-to-water heat pump satisfies this requirement and for this reason was selected as a system in which flammable refrigerants were evaluated.

Didion (Mulroy et al; 1988) originally proposed the use of zeotropic mixtures in the water-to-water heat pump as a method for improving heat pump performance for low-lift/high-glide applications. A later simulation study showed that the Coefficient of Performance (COP) of the water-to-water system charged with a zeotropic mixture can approach the COP of the direct-expansion R22 system if large counter-flow heat exchangers are used as the evaporator and condenser (Domanski et al., 1994). The follow-up experiment in a general-purpose mini-breadboard heat pump (MBHP) showed the importance of adequate sizing of the heat exchangers (Choi et al., 1996). The evaporator and condenser of the MBHP did not have sufficient capacity to obtain a sizable gain in COP due to glide matching between the zeotropic mixture and heat-transfer fluid. The current study was performed in a specially designed apparatus with a large brazed plate evaporator and condenser to ensure adequate capacity.

2: Experimental Setup

The experimental setup consisted of four main subsystems; the vapor-compression system, the indoor heat transfer fluid loop, the outdoor heat transfer fluid loop, and the ground loop.

2.1: Refrigerant Cycle

Figure 2.1 shows a schematic of the vapor-compression system. The system consisted of a reciprocating compressor, condenser, a manually adjustable expansion device, evaporator, and an accumulator. The compressor was a two-cylinder, open-drive reciprocating design displacing from 3.53 m^3/h (2.08 cfm) to 21.76 m^3/h (12.81 cfm) with minimum speed of 500 rpm and maximum speed of 3000 rpm. Compressor bore was 55 mm (2.16 in) and stroke was 49 mm (1.93 in). The brazed plate heat exchanger was installed to provide for counter-flow heat exchange between the refrigerant and a 70 %/30 % by mass water/ethylene glycol heat transfer fluid. The system was designed for a cooling load of 10.6 kW (36000 Btu/h). The high pressure refrigerant tubing was copper with 12.7 mm OD (0.5 in) and 9.5 mm ID (0.375 in). The low pressure refrigerant tubing was copper with 15.9 mm OD (0.625 in) and 12.7 mm ID (0.5 in).

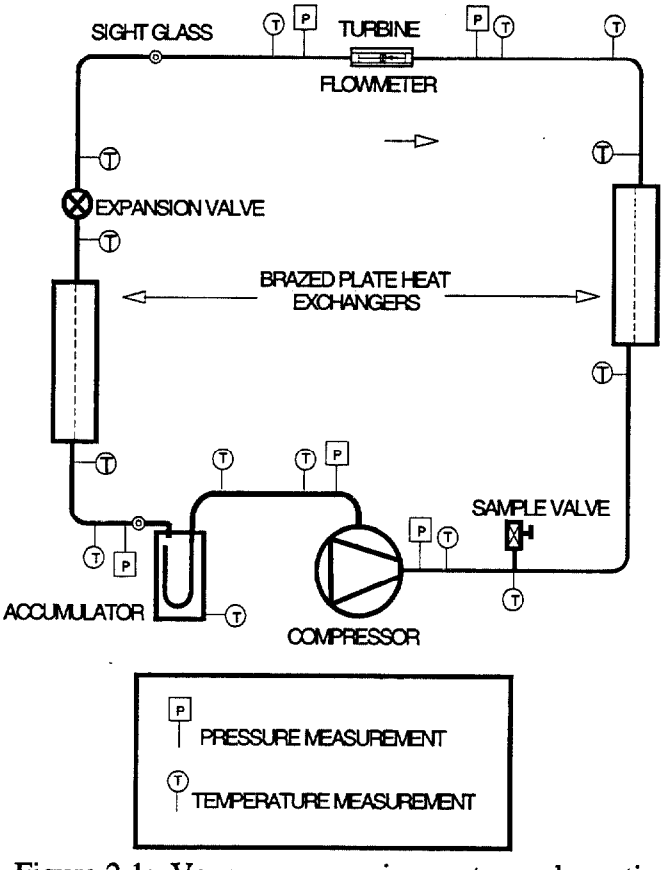

Figure 2.1: Vapor-compression system schematic

The compressor was driven by a 11.2 kW (15 hp) explosion-proof motor coupled to the compressor shaft through a torque and RPM transducer. The motor speed was controlled by a variable frequency drive. The motor was oversized to compensate for the loss of torque at high frequency. The use of an open drive compressor removed the motor power consumption from COP calculations and did not effect vapor superheat entering the compression cylinders.

2.2: Indoor and Outdoor Heat Transfer Fluid Loops

The vapor-compression refrigeration system communicated with its heat source and sink using ethylene glycol water heat transfer fluid (HTF) in counter-flow through brazed plate heat exchangers. The system was configured to allow the HTF to remain in counter-flow in both the heating and cooling modes. During cooling operation the evaporator HTF was diverted to the indoor air coil, and in the heating mode the condenser HTF was diverted to the indoor air coil. Figure 2.2 shows the arrangement of the HTF piping and all relevant measurement points.

The HTF temperature changes were measured by 10-junction thermopiles located in oil filled wells in the copper HTF lines. Thermopiles were located across the evaporator, condenser, and ground heat exchangers. A 25-junction thermopile measured the air temperature change, and dewpoint instruments measured the change of moisture content across the finned tube air coil. HTF density and specific heat values were supplied by the fluid manufacturer (Dow 1995).

Centrifugal pumps circulated the HTF. The indoor and outdoor HTF loops contained expansion tanks open to atmospheric pressure. Expansion volume was necessary due to the large changes in temperature that occurred between heating and cooling conditions. The HTF flowrates were controlled using ball valves as throttling devices. Maximum volumetric flowrate was 34.1 l/min (9 gpm). Filter assemblies in both loops provided for sediment removal.

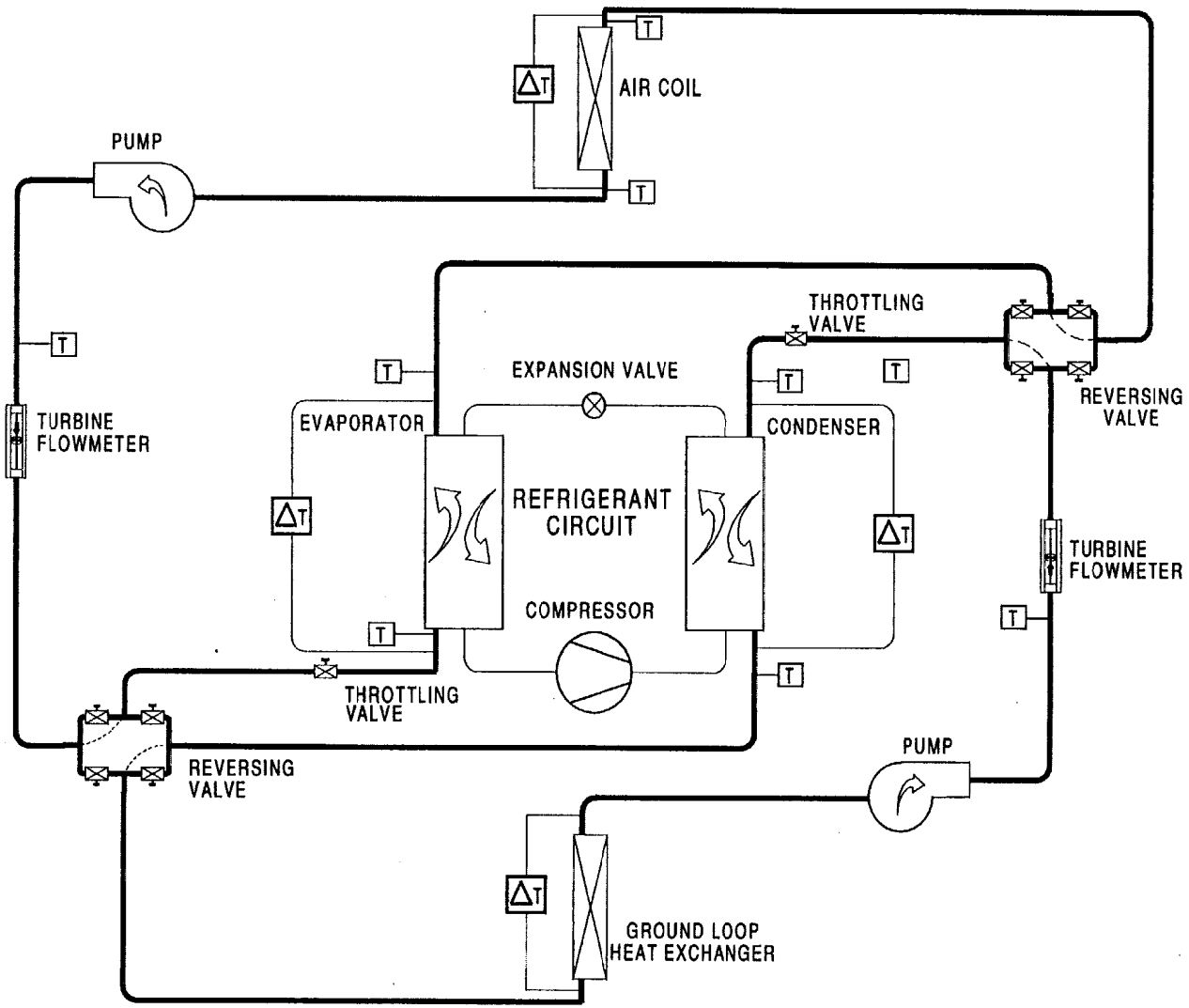

Figure 2.2: Configuration of heat transfer fluid loops in the cooling mode

2.3: Ground Heat Transfer Fluid Loop

A brazed plate heat exchanger was used to transfer heat between the indoor/outdoor HTF loop and the ground HTF loop. Temperature of the ground HTF was controlled for heating and cooling conditions. Figure 2.3 shows the major components of the ground HTF loop.

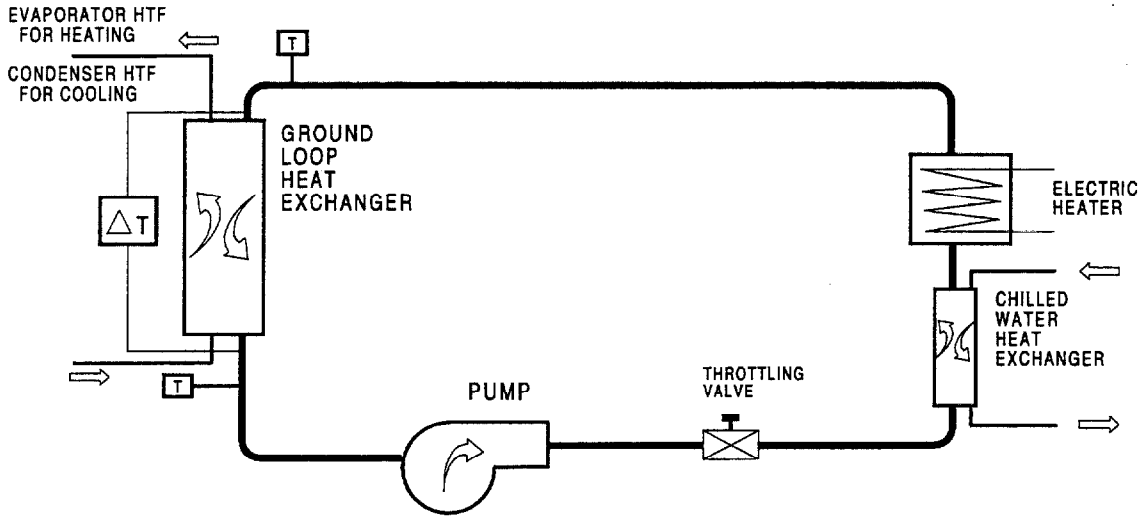

Figure 2.3: Ground heat transfer fluid loop schematic

The ground loop HTF was circulated by a centrifugal pump at a maximum rate of 37.9 l/min (10 gpm). After passing through the pump, the HTF entered a small brazed plate heat exchanger to transfer heat with chilled water supplied at approximately 5.6 °C (42 °F). This cooled the HTF slightly below the desired setpoint temperature. The HTF was then reheated by flowing over an insertion type electric resistance heating element of approximately 10 kW (34121 Btu/h) maximum output. The electric resistance heating element was powered by 240 VAC passing through an SCR (silicon controlled rectifier). The data acquisition set the SCR output using a 4 mA to 20 mA DC signal.

2.4: Instrumentation and Data Acquisition

Data were gathered using a data acquisition unit controlled by a personal computer. The 130 measurement points consisted of temperature, pressure, pressure difference, temperature difference, dewpoint temperature, torque, RPM, and frequency. Refrigerant composition was determined by gas chromatography of refrigerant samples taken from the compressor discharge. Table 2.1 lists measured quantities and their 95 % confidence limits. Appendix A gives a detailed uncertainty analysis for capacity, COP and other quantities.

Table 2.1: Instrumentation uncertainty

Quantity	Range	Uncertainty
Pressure	0 kPa –3447 kPa (0 psia – 500 psia)	±3.4 kPa (±0.5 psia)
Temperature	-26.1 °C - 93.3 °C (-15 °F – 200 °F)	±0.3 °C (±0.5 °F)
Temperature Difference	0 °C – 27.8 °C (0 °F – 50 °F)	±0.3 °C (±0.5 °F)
Barometric Pressure	0 mm Hg - 1270 mm Hg (0 in Hg - 50 in Hg)	±0.34 mm Hg (±0.0135 in Hg)
Dewpoint Temperature	0 °C – 50 °C (32 °F – 122 °F)	±0.2 °C (±0.4 °F)
Refrigerant Concentration	0 – 100 % mass	±1.0 %
Pressure Difference	0 Pa – 1244 Pa (0 in H_2O - 5 in H_2O)	±24.4 Pa (±0.098 in H_2O)
Frequency	0 kHz - 5 kHz	±2.1 Hz
Torque	0 N-m - 39.54 N-m (0 in-lbf – 350 in-lbf)	±1 %
RPM	500 RPM – 3000 RPM	±5 RPM
Volumetric Flow	0 lpm - 37.9 lpm (0 gpm - 10 gpm)	±1 %

3: Experimental Procedure

3.1: Test Procedure

In the cooling mode the indoor HTF passed through the refrigerant evaporator where it was cooled and pumped to the indoor finned tube air coil. The outdoor loop HTF was in contact with the ground heat exchanger and the refrigerant condenser. Table 3.1 lists the cooling conditions under which data were captured. Indoor conditions and HTF temperatures were established according to ARI Standard 330 (ARI 1993).

Table 3.1: Cooling test conditions

Location	Setpoint	Tolerance
Indoor Dry-bulb Temperature	26.7 °C (80.0 °F)	±0.3 °C (±0.5 °F)
Indoor Dewpoint Temperature	15.8 °C (60.4 °F)	±0.3 °C (±0.5 °F)
Condenser HTF Inlet Temperature	25.0 °C (77.0 °F)	±0.3 °C (±0.5 °F)
HTF Temperature Differences Across the Evaporator and Condenser	5.6 °C (10.0 °F)	±0.3 °C (±0.5 °F)
Refrigerant Evaporator Superheat and Condenser Subcooling	3.9 °C (7.0 °F)	±1.1 °C (±2.0 °F)

The water-to-water heat pump rig was energized with the compressor operating at 1500 RPM to rapidly circulate refrigerant and clear the lines and heat exchangers of oil that could have migrated during previous tests. Once the compressor sump oil level reached its highest mark, the compressor RPM would be adjusted to the desired RPM while pump speeds, expansion devices, and loop parameters were adjusted to meet the test conditions. The psychrometric room setpoints were continuously monitored and adjusted to compensate for the change in heating or cooling loads upon test rig start-up. Indoor air coil air flowrate was monitored and adjusted to produce a 11.1 °C (20.0 °F) temperature difference across the coil. The air coil valves were adjusted to produce a two-row cross counter-flow pattern with HTF first entering the downstream row.

The system operated in the cooling mode for several hours to allow the air coil to produce a consistent flow of condensate. Condensate flow was monitored with a load cell.

Comparisons were continuously made between air-side capacity calculated from air enthalpy change and air-side capacity calculated from the HTF energy change. The steady-state capacity measurements agreed to within 3.5 %. Air flow patterns through the air coil were monitored by 25 junction thermocouple grids upstream and downstream of the coils. If temperatures across the airstream deviated by more the 0.17 °C (0.3 °F), an additional air mixing fan was adjusted at the air tunnel entrance to more thoroughly mix the inlet air.

Refrigerant conditions were monitored and adjusted to produce 3.9 °C (7.0 °F) superheat and subcooling at the evaporator and condenser exits, respectively. These adjustments were accomplished by changing the system charge and adjusting the expansion valves. Once proper superheat and subcooling conditions were established, the system was operated without adjustment to verify stability of both the system and the psychrometric room. With steady-state conditions satisfied the composition of the refrigerant charge would be verified by sampling from the compressor discharge line. The sample would then be analyzed in the gas chromatograph. Previous calibrations of the gas chromatograph produced composition measurements with an expanded uncertainty of 1.0 % at the 95 % confidence level.

R22 was first tested in the water-to-water system to establish the conditions for the direct expansion test cases. For the direct expansion cooling simulations, the saturation temperature of R22 in the evaporator was controlled to match the average HTF temperature across the air coil during the water-to-water cooling tests. Water-to-air heating tests were conducted in a similar manner with the condenser saturation temperature matching the average air-coil HTF temperature during a water-to-water heating test. These direct expansion simulations reduced the pressure ratio across the compressor and decreased the temperature lift for the cooling/heating process. These water-to-air heat pump tests were conducted to provide an indication as to what extent glide matching between the indoor HTF and zeotropic mixture could mitigate the penalty associated with the indoor-loop HTF/refrigerant heat exchanger needed to isolate flammable refrigerants outdoors.

During the heating mode the reversing valves were set to direct the refrigerant condenser HTF flow to the indoor air coil and the refrigerant evaporator HTF flow to the ground heat exchanger. The flowrates of HTF in the air coil and ground loop heat exchanger were the same as during the cooling mode operation. This meant that the HTF flowrate seen by the condenser during the cooling test would now be seen by the evaporator during the heating test. This criteria was established for all heating tests to mimic the performance of a reversing valve arrangement for the HTF in both indoor and outdoor loops. It also meant that the temperature glide established for the cooling tests would no longer be applicable for the heating tests. Heating HTF temperature glides were established by energy considerations in both heat exchangers. Heating HTF temperature changes were determined by internal heat transfer coefficients and an energy balance between the refrigerant and HTF sides of each heat exchanger. Table 3.2 lists the heating conditions under which data were captured.

Table 3.2: Heating test conditions

Location	Setpoint	Tolerance
Indoor Dry-bulb Temperature	21.1 °C (70.0 °F)	±0.3 °C (±0.5 °F)
Indoor Dewpoint Temperature	12.06 °C (53.7 °F) maximum	±0.3 °C (±0.5 °F)
Evaporator HTF Inlet Temperature	0.0 °C (32.0 °F)	±0.3 °C (±0.5 °F)
HTF Temperature Differences Across the Evaporator and Condenser	NA	NA
Refrigerant Evaporator Superheat and Condenser Subcooling	3.9 °C (7.0 °F)	±1.7 °C (±3.0 °F)

3.2: Refrigerants Tested

Table 3.3 lists the tested refrigerants and their selected properties. The compositions of the different refrigerants were chosen using simulations performed with CYCLE-11 (Domanski and McLinden 1992). The UA version of CYCLE-11 was used for all simulations. The composition were chosen to maximize COP for the given simulation conditions.

ANSI/ASHRAE Standard 34-1992 (1992) assigns a safety group to each refrigerant given as A1 for R22, A3 for R290, A2/A3 for R32/290, A2/A2 for R32/152a, and A3/A3 for R290/600a. The "A" designation indicates that toxicity has not been identified for these refrigerants at concentrations below 400 x 10^{-6}. The number 1 indicates no flame propagation occurs in air at 101 kPa (14.7 psia) and 21 °C (70 °F), 2 indicates a lower flammability limit of more than 0.10 kg/m^3 (0.00625 lb/ft^3) and a heat of combustion less than 19000 kJ/kg (8174 Btu/lb), and 3 indicates that the refrigerant is highly flammable at a concentration of less than 2 with a heat of combustion greater than 19000 kJ/kg (8174 Btu/lb).

Table 3.3: Selected properties of tested refrigerants at 4.4 °C (40 °F) saturation temperature[a]

Name	GWP[b]	ASHRAE Standard 34 Safety Group	Vapor Pressure [c] kPa (psia)	T_{dew} - T_{bub} °C, (°F) [c]	Liquid Thermal Conductivity W/(m °C) (Btu/(h ft °F))	Vapor Absolute Viscosity kg/(m s) (lb/(ft h))	Volumetric Capacity kJ/m^3 ($Btu/(ft^3)$)
R22	1500	A1	574.3 (83.3)	0	0.09467 (0.0547)	11.891×10^{-6} (.02873)	4895.8 (131.4)
R290	20	A3	541.9 (78.6)	0	0.10395 (0.06006)	7.81836×10^{-6} (0.01889)	4344.4 (116.6)
R32/290 (50/50)	335	A2 / A3	976.9 (141.69)	5.7 (10.3)	0.12015 (0.06942)	9.70569×10^{-6} (.02345)	8532.3 (229.0)
R32/152a (50/50)	395	A2 / A2	551.6 (80.0)	7.9 (14.2)	0.13062 (0.07547)	1.05707×10^{-6} (.02554)	5059.8 (135.8)
R290/600a (70/30)	20	A3 / A3	415.4 (60.25)	6.6 (11.9)	0.10516 (0.06076)	7.599×10^{-6} (0.01836)	3524.7 (94.6)

[a] From REFPROP 5.16 (NIST 1996)

[b] integrated time horizon 100 years; CO_2 as reference

[c] zeotropic mixture pressure at a 4.4 °C (40 °F) average of dew and bubble temperatures

4: Experimental Results

4.1: Performance as a function of compressor speed

Figure 4.1 shows that the cooling capacity of the R32/290 mixture was greater than the other refrigerants for all RPM. At 1000 RPM the cooling capacity of R32/290 ranged from 31 % to 117 % higher than the other refrigerants. The high capacity of the R32/290 mixture would be expected from its higher pressure and its higher volumetric cooling capacity. Table 4.1 summarizes volumetric cooling capacities of the different refrigerants at an evaporating temperature of 4.4 °C (40 °F) and evaporator inlet quality of 25 %. The saturation pressure and volumetric capacity of the R32/290 mixture exceeded that of R22 by 77 % and 55 %, respectively.

Figure 4.2 shows the heating capacity of the various refrigerants as a function of RPM. Refer to Appendix A, Section A.4 for uncertainty analysis. The relatively large volumetric capacity of R32/290 produced higher heating capacity than the other refrigerants and 42 % higher than the R22-REF tests. When compared to the R22-REF test at 1000 RPM, R290 was 10 % lower while R32/290 was 57 % higher. The addition of isobutane to the pure propane caused a 26 % decrease in heating capacity compared to pure R290. This decrease in capacity with the addition of isobutane corresponds to the 29 % lower volumetric capacity of the R290/600a mixture at the heating conditions.

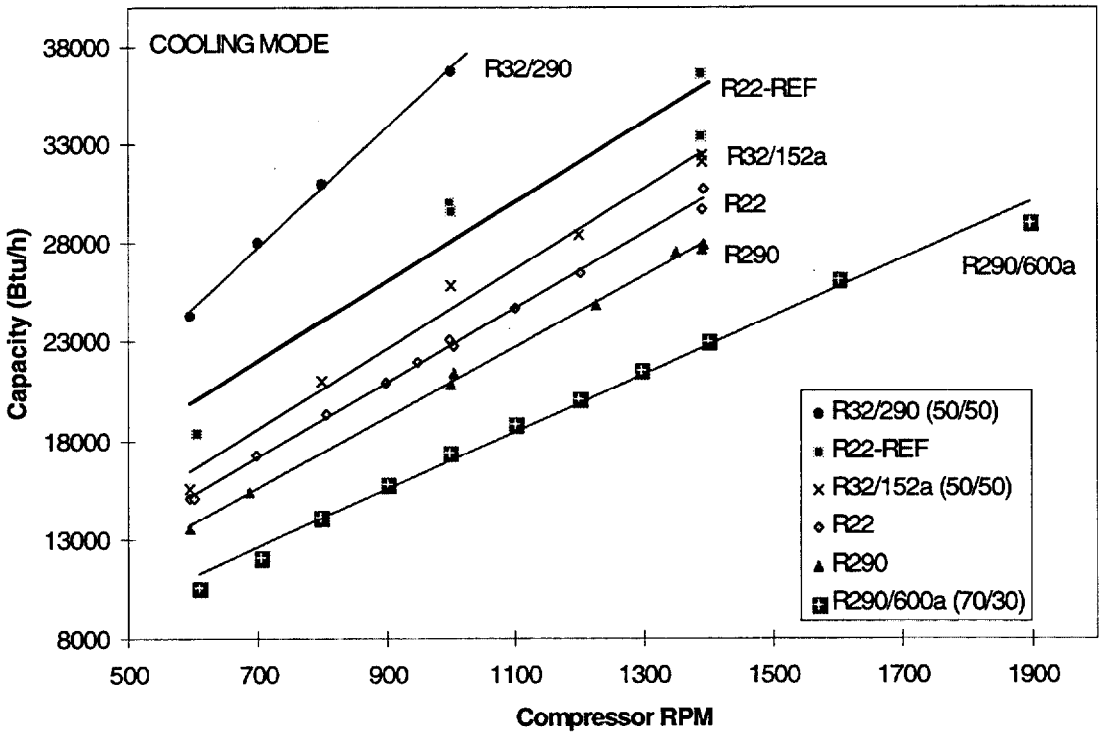

Figure 4.1: Cooling capacity as a function of compressor RPM

Table 4.1: Volumetric Capacity comparison at 4.4 °C(40 °F) evaporating conditions*

Refrigerant	Saturated Vapor Pressure KPa, (psia)	Saturated Vapor Density kg/m^3, (lbm/ft^3)	Enthalpy of Vaporization kJ/kg, (Btu/lbm)	Volumetric Capacity at 25 % Inlet Quality kJ/m^3, (Btu/ft^3)
R32/290 (50/50)	979.7 (142.10)	22.9 (1.428)	330.6 (142.13)	5681.7 (152.21)
R32/152a (50/50)	554.5 (80.42)	13.5 (0.8412)	322.0 (138.45)	3260.6 (87.35)
R22	574.0 (83.25)	24.6 (1.535)	199.0 (85.55)	3676.1 (98.48)
R290	542.1 (78.62)	11.8 (0.7361)	368.2 (158.31)	3264.0 (87.44)
R290/600a (70/30)	416.4 (60.39)	8.7 (0.5460)	357.8 (153.82)	3135.2 (83.99)

*Properties found with REFPROP 5.16

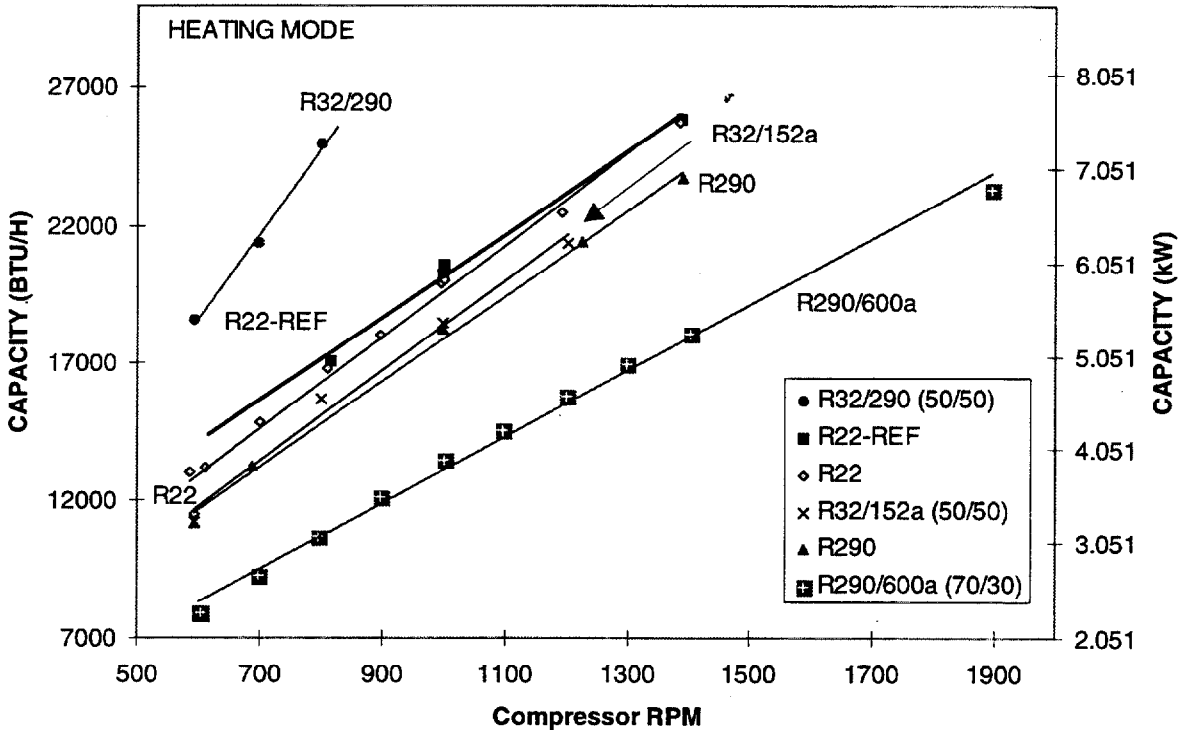

Figure 4.2: Heating capacity as a function of compressor RPM

4.2: COP at a constant capacity

Figure 4.3 shows COP and RPM at a constant cooling capacity of 8.5 kW (29003 Btu/h) for all of the refrigerants. The same evaporator heat flux is present in all cases, which is in keeping with recommendations made by McLinden and Radermacher (1987). The figure shows that R290/600a must be circulated 74 % more than R22-REF to produce the same cooling capacity. R32/290 produced the same cooling capacity as R22-REF with 29 % lower compressor RPM. R290 and R32/152a had compressor RPMs that were 40 % and 16 % higher than R22-REF, respectively.

Figure 4.3 also compares COP of the refrigerants relative to the R22-REF case. COP was calculated based upon measured shaft power and air side capacity. The figure shows that all of the flammable refrigerants performed at least as well as R22. An uncertainty of 3 % in COP is achieved at this capacity. R32/290 cooling COP was 12 % below the R22-REF case. R290 and R32/152a were within 17 % and 18 % of R22-REF, respectively. R290/600a and R22 had comparable COPs.

Figure 4.4 shows cooling COP over a wide range of cooling capacities. Refer to Appendix A, Section A.5 for all COP uncertainty analyses. R32/290 produced the highest cooling COP of the alternate refrigerants and averaged 11 % lower than R22-REF over its range of tested cooling capacity. Over the range of cooling capacities tested for R32/290, its COP averaged 17 % higher than R22 in the water-to-water configuration. There was no significant difference in cooling COP between R290 and R32/152a for the same compressor speed. R290 averaged 9 % higher cooling COP than R22 over its tested capacity range. R290/600a and R22 were not significantly different over the tested capacity range until a capacity of approximately 8.6 kW (30000 Btu/h). Here they diverged with increasing capacity, but both COP measurements had overlapping uncertainty bands.

Figure 4.5 shows the heating performance relative to R22-REF at a constant heating capacity of 6.5 kW (22179 Btu/h). Here again the amount of refrigerant circulated corresponds to the volumetric cooling capacity. The COP of all of the refrigerants approach R22-REF within 20 %. This is due to the nature of the heating tests. For the heating tests the condenser conditions were varied. All of the refrigerants, including R22-REF, had evaporating temperatures that were within ±2.2 °C (4 °F).

Figure 4.6 shows that the performance of the refrigerants was much closer than the cooling tests. This was due to the similar evaporator conditions. R290 was within 4 % of the COP of the R22-REF tests over the entire capacity range. R290 outperformed R22 in the water-to-water configuration by 5 %. This would seem to indicate the influence of the better transport properties of R290. R32/152a and R32/290 were within 6 % over the capacity range shown. R32/290 heating COP averaged 3 % lower than R22 and 10 % lower than R22-REF. R290/600a was not able to meet the performance of the R32/152a as it did during the cooling tests. The lower volumetric capacity of the R290/600a mixture meant that higher RPMs were needed, which produced lower COP.

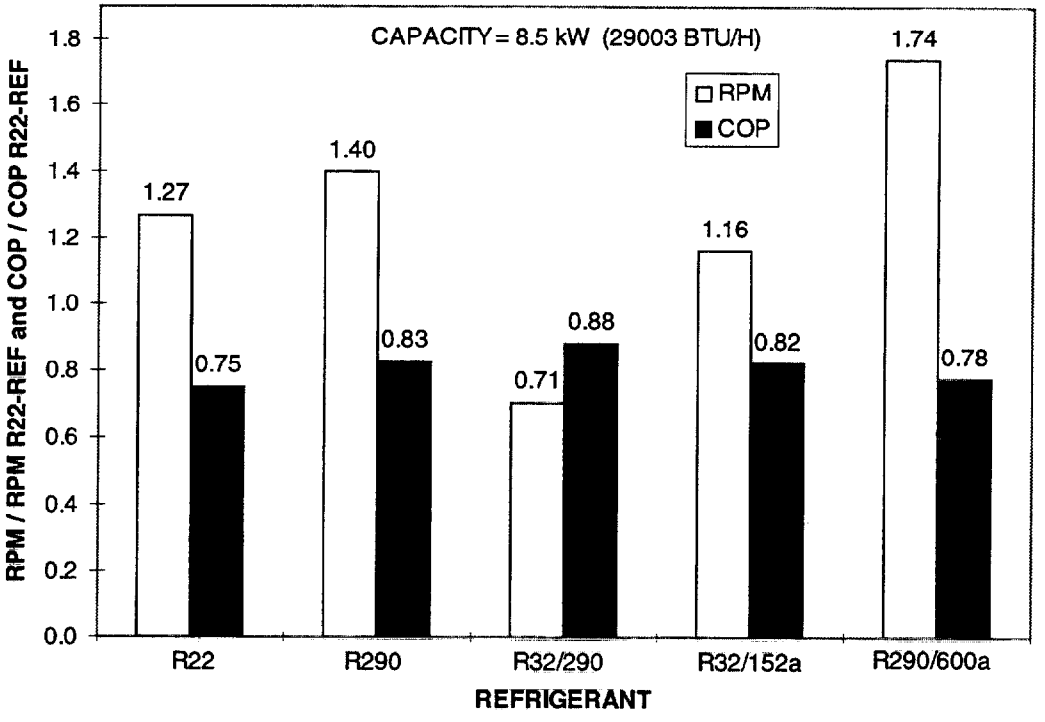

Figure 4.3: Cooling COP and RPM at constant capacity

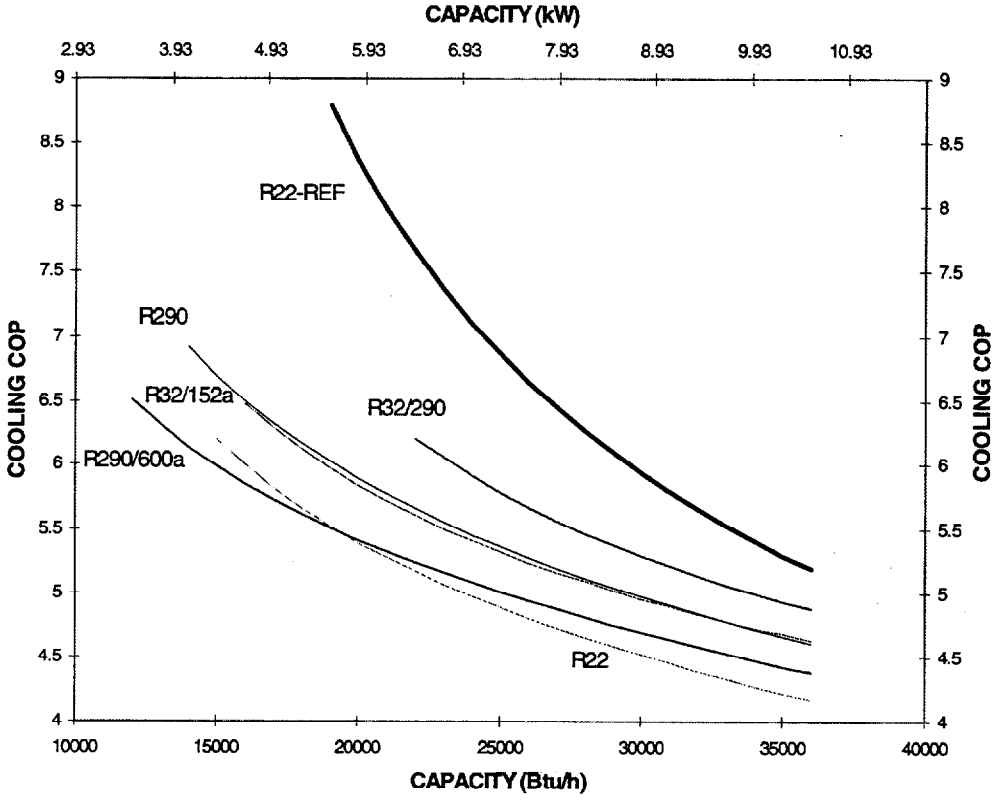

Figure 4.4: Cooling COP as a function of capacity

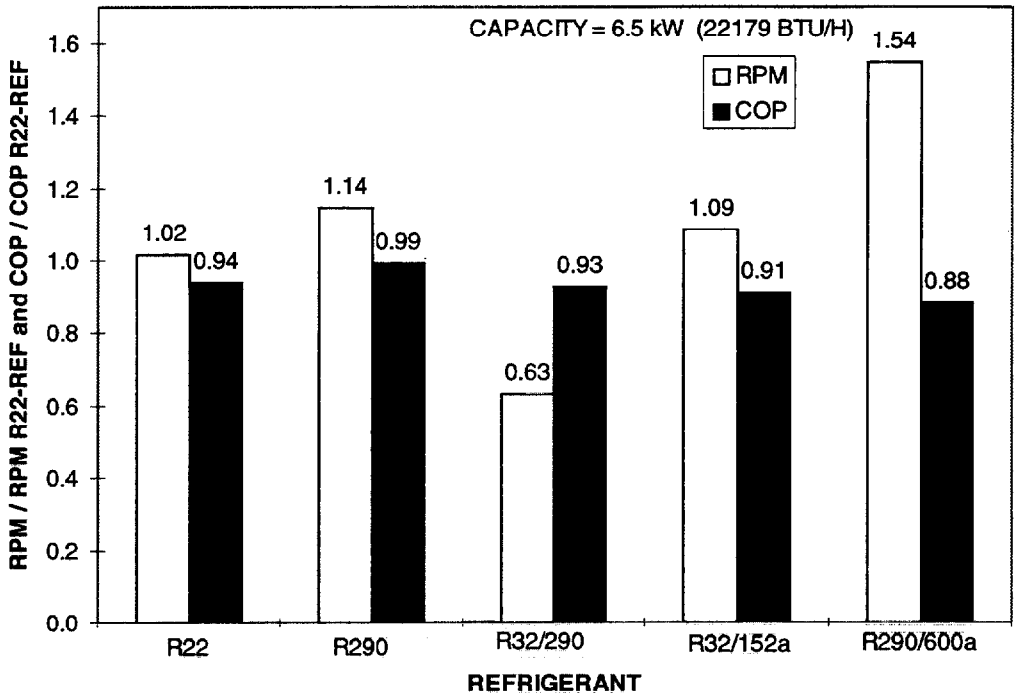

Figure 4.5: Heating COP and RPM at constant capacity

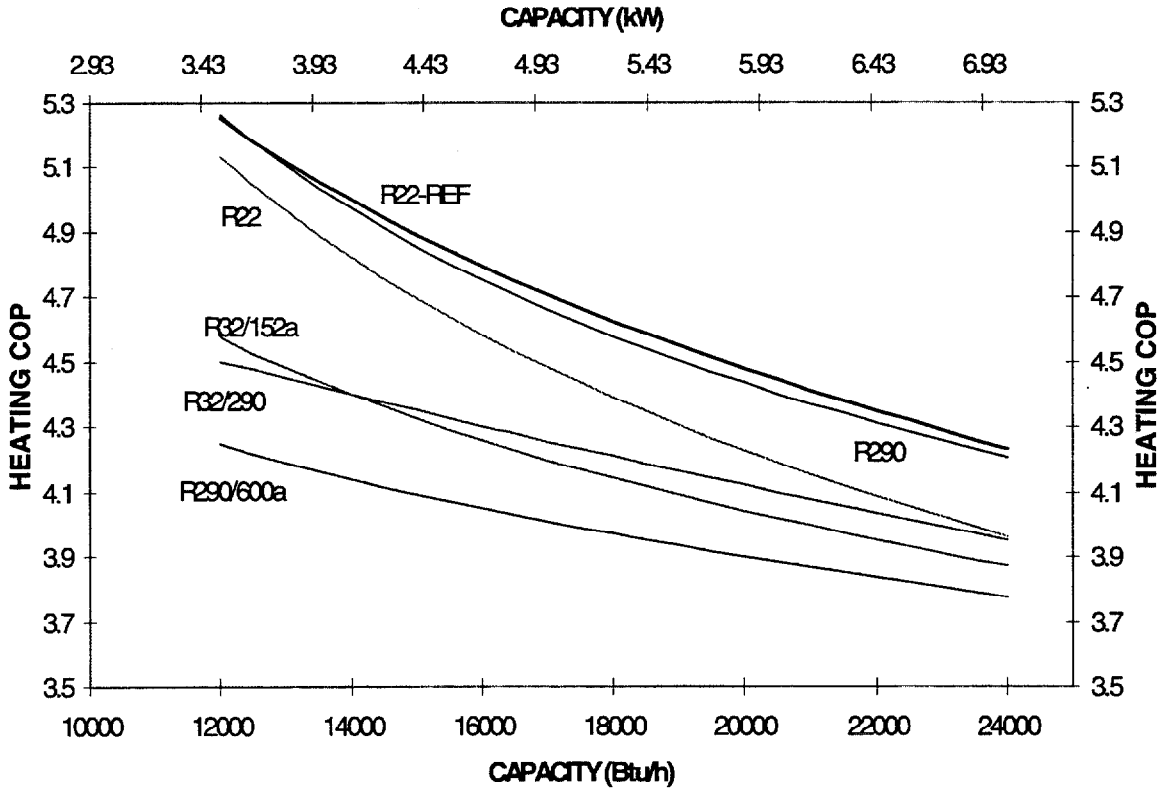

Figure 4.6: Heating COP as a function of capacity

4.3: Glide Matching

Condenser refrigerant temperature glides were based upon the saturated vapor and liquid temperatures at the inlet and exit, respectively. In the evaporator the temperature glides were based upon the measured refrigerant temperature at the two-phase exit of the expansion device and the saturated vapor temperature at the evaporator exit pressure. All superheated and subcooled portions of the refrigerant path were neglected for temperature glide and log-mean temperature difference (LMTD) calculations.

Table 4.2 shows glide matching and LMTD results for the cooling tests at a constant capacity of 8.5 kW (29003 Btu/h). The HTF had a temperature change of 5.6 °C (10.0 °F) through the evaporator and condenser. The pure refrigerants underglided the HTF while the zeotropic mixtures all overglided with the exception of R290/600a, which underglided in the evaporator.

Cooling log-mean temperature differences (LMTDs) for the R22-REF case were less than 2.0 °C (3.6 °F) due to the increased evaporating temperature. R22, R290, and R32/152a produced similar average evaporator LMTDs near 5.6 °C (10.0 °F) ± 0.2 °C (0.4 °F). In the condenser R22 and R290 had LMTDs of 4.4 °C (8.0 °F) while the other refrigerants were 1.1 °C (2.0 °F) to 2.9 °C (5.3 °F) higher.

Heating tests were more difficult to quantify due to the varying HTF glide. During the heating tests the HTF volumetric flowrates were set equal to their values during the same RPM cooling tests. Cooling evaporator volumetric flowrate was seen in the heating condenser, and cooling condenser flowrate was seen in the heating evaporator. This switch in volumetric flows was used to more closely approximate a field installation. This did not produce the 5.6 °C (10.0 °F) temperature glide seen during the cooling tests. Table 4.3 shows the glide matching and LMTD results at a constant heating capacity of 6.5 kW (22179 Btu/h). The table shows that evaporator heating glides corresponded with those seen in cooling; the pure refrigerant tests underglided and the zeotropes overglided. Condenser glides showed the same undergliding and overgliding behavior.

Heating average evaporator LMTDs were consistently smaller for R22 and R290 ranging from 3.9 °C (7.0 °F) for R22 to 4.0 °C (7.2 °F) for R290. Smaller LMTDs were due to the higher evaporator volumetric flowrate per unit capacity seen during the heating tests. Condenser LMTDs ranged from 2.0 °C (3.6 °F) to 2.3 °C (4.2 °F) for the pure refrigerants and from 4.4 °C (8.3 °F) to 6.3 °C (11.4 °F) for the zeotropes.

Table 4.2: Cooling LMTD and refrigerant glide matching [a,b]

	R22-REF	R22	R290	R32/290	R32/152a	R290/600a
Evaporator Glide °C (°F)	-1.2 (-2.1)	-1.4 (-2.6)	-1.1 (-1.9)	7.2 (12.9)	7.3 (13.1)	3.4 (6.1)
Condenser Glide °C (°F)	-1.6 (-2.8)	-1.9 (-3.5)	-1.1 (-1.9)	-7.4 (-13.3)	-7.2 (-13.0)	-7.4 (-13.3)
Evaporator LMTD °C (°F)	1.2 (2.1)	6.7 (12.0)	6.1 (11.0)	4.1 (7.4)	5.6 (10.0)	4.2 (7.6)
Condenser LMTD °C (°F)	1.6 (2.9)	4.4 (8.0)	4.4 (8.0)	7.4 (13.3)	6.6 (11.9)	5.6 (10.0)

a-- Glide = $T_{out} - T_{in}$ b—Linear interpolation at 8.5 kW (29003 Btu/h).

Table 4.3: Heating LMTD and refrigerant glide matching [c]

	R22-REF	R22	R290	R32/290	R32/152a	R290/600a
Evaporator Glide °C (°F)	-1.5 (-2.7)	-1.4 (-2.5)	-1.2 (-2.2)	6.4 (11.6)	6.2 (11.1)	2.4 (4.4)
Condenser Glide °C (°F)	-1.3 (-2.3)	-0.4 (-0.7)	-0.4 (-0.7)	-6.9 (-12.5)	-7.4 (-13.4)	-6.0 (-10.8)
Evaporator LMTD °C (°F)	4.8 (8.6)	4.8 (8.6)	4.3 (7.8)	4.9 (8.8)	6.7 (12.1)	3.8 (6.8)
Condenser LMTD °C (°F)	2.2 (3.9)	2.5 (4.5)	2.7 (4.9)	6.3 (11.4)	4.9 (8.8)	4.6 (8.3)
HTF Glide Evap / Cond °C (°F)	-2.8 (-5.7) / 4.1 (7.3)	-3.0 (-5.4) / 4.2 (7.5)	-2.9 (-5.3) / 4.2 (7.6)	-2.8 (-5.0) / 3.9 (7.0)	-2.6 (-4.6) / 3.7 (6.7)	-2.6 (-4.6) / 4.0 (7.2)

c—Linear interpolation at 6.5 kW (22179 Btu/h)

5: Concluding Remarks

The goal of this study was to examine the concept of the water-to-water heat pump with reference to a direct expansion air-to-air system. Specifically, the study investigated to what degree the excellent transport properties of flammable refrigerants and glide matching between HTF and the selected zeotropic mixtures could mitigate the performance loss caused by the use of the indoor HTF loop. The zeotropic refrigerants tested in this work did allow the refrigerant temperature to more closely match the temperature of the heat transfer fluid, but this improvement in performance relative to R22 did not overcome the penalty of the added HTF loop.

In the cooling mode tests, R22 in the water-to-water configuration showed a 25 % penalty in COP due to the added temperature lift of the extra HTF loop. The flammable zeotrope, R32/290 (50/50), was able to remove almost half of this deficiency, but still produced a 12 % lower COP than the R22-REF case. Propane (R290) was able to exceed the performance of R22 throughout the capacity range tested. This was due to propane's transport and thermodynamic properties. The lower pressure ratio, suction line viscosity, and evaporator LMTD seen with propane contributed to its performance improvements over R22. Similar arguments could be made for the other zeotropes containing R32 and hydrocarbons; improved transport properties produced lower average LMTDs in the evaporator and contributed to improvement in performance relative to R22.

In the heating mode tests, the refrigerants were much more closely matched due to the similar evaporating conditions and the higher temperature lift. Propane approached the performance of R22-REF due to the similar evaporating conditions. The R290/600a mixture performance decreased much more in the heating tests relative to its cooling performance. This was due to the lower volumetric capacity, higher pressure ratio, and higher LMTD in the condenser compared to R22. R32/290 and R32/152a posted COPs that were 6 % below the R22-REF case. Since glide matching was controlled in the cooling mode only, a glide match was not obtained in heating.

If we include the penalty of pumping power in the COP calculation, all of the refrigerants suffer a 5 % degradation. This is assuming a loss rate of 3.6 W/lpm (13.6 W/gpm) (ARI 1993). This would lower the performance of the R32/290 system to approximately 18 % below that of the R22-REF water-to-air system. R32/290 in the heating mode has the potential to match the performance of the R22-REF system if HTF flowrates were optimized. As tested the pure refrigerant, R290 (propane), performed well in both heating and cooling.

If the main function of the water-to-water heat pump was hydronic heating and cooling, then the R32/290 mixture showed the best cooling COP, which was greater by 6 % to 9 % than the COPs of R32/152a, R290, R290/600a, and R22. R32/290 COP was helped by good glide matching and higher volumetric capacity relative to the other refrigerants. In the heating mode the performance of R290 was the best.

Further improvements in the COP of a water-to-water heat pump require lowering the LMTD in the evaporator and condenser below about 5 °C (8 °F). Small temperature differences require large heat exchangers. Low pressure drop requires lower fluid velocity at the expense of lower HTF side heat transfer coefficients which reduces the capacity of the heat exchanger. A system designer will optimize these conflicting constraints based upon economics and desired system performance. An additional difficulty with attaining lower temperature differences in the heat exchangers is the few degrees of evaporator superheat and condenser subcooling present in vapor compression systems. An intra-cycle heat exchanger that allows two-phase vapor to exit the condenser and subcool low quality refrigerant leaving the condenser would allow lower temperature differences. For zeotropic mixtures this kind of heat transfer would increase evaporator pressure and improve COP.

References

Alefeld, G. 1987. Efficiency of compressor heat pumps and refrigerators derived from the second law of thermodynamics. *International Journal of Refrigeration.* Vol. 10 No.6. pp. 331-341.

Albritton, D.L., 1998. Ozone Depletion and Global Warming, Proceedings of ASHRAE/NIST Refrigerants Conference "Refrigerants for the 21st Century", Gaithersburg, MD, pp. 1-5.

ANSI/ASHRAE Standard 34-1992. *Number designation and safety classification of refrigerants.* American Society of Heating, Refrigerating and Air-Conditioning Engineers. 1791 Tullie Circle NE, Atlanta, GA, USA.

ARI. 1993. *Standard for ground source closed-loop heat pumps: Standard 330.* Air-conditioning and Refrigeration Institute. 4301 North Fairfax Drive, Arlington, Virginia USA, 22203.

ASHRAE Standard 116-1983. *Method of testing for seasonal efficiency of unitary air-conditioners and heat pumps.* American Society of Heating, Refrigerating and Air-Conditioning Engineers. 1791 Tullie Circle NE, Atlanta, GA, USA.

Bivens, D. B., D. M. Patron, and A. Yokozeki. 1997. Performance of R-32/R-125/R-134a mixtures in systems with accumulators or flooded evaporators. *ASHRAE Transactions* 103(1).

Calm, J. M. 1993. Comparative global warming impacts of electric vapor-compression and direct-fired absorption equipment. *Report TR-103297.* Electric Power Research Institute (EPRI). Palo Alto, CA USA.

Choi, D. K., P. A. Domanski, and D. A. Didion. 1996. Evaluation of flammable refrigerants for use in a water-to-water residential heat pump. IIF – IIR Commissions B1, B2, E1, and E2 Conference. *Applications for natural refrigerants.* Aarhus, Denmark. September 3-6.

Domanski, P. A. and M. O. McLinden. 1992. A simplified cycle simulation model for the performance rating of refrigerants and refrigerant mixtures. *International Journal of Refrigeration.* Vol. 15 No.2. pp. 81-88.

Domanski, P. A., D. A. Didion, and W. Mulroy. 1994. A simulation model and study of hydrocarbon refrigerants for residential heat pump systems. IIR Conference, Hanover, Germany, pp. 339-354.

Dow Chemical Company. 1995. Fluidfile 2.0 software program for Windows. Midland, Michigan, USA.

Grob, D. P. 1997. Use of flammable refrigerants: safety standards and risk analysis. *Compression systems with natural working fluids.* Annex 22. HPP-AN22-3. Gatlinburg, Tennessee, USA. October. 49-61.

Halozan, H. 1995. Practical experience with direct-expansion propane heat pumps in Austria. *Compression systems with natural working fluids: applications, experience and developments.* Annex 22. IEA. HPP-AN22-1. Trondheim, Norway. October. 131-143.

Herold, K.E. 1989. Performance limits for thermodynamic cycles. Proceedings of the Heat Pump Symposium at the ASME Winter Annual Meeting, San Francisco,California, AES-Vol. 7. pp. 15-22.

Kim, M. S., G. Morrison, W. J. Mulroy, and D. A. Didion. 1996. A study to determine the existence of an azeotropic R-22 'drop in' substitute. NISTIR 5784. National Institute of Standards and Technology. Gaithersburg, MD. USA.

Lystad, Tor. 1995. Testing of a heat pump with propane as working fluid. *Compression systems with natural working fluids: applications, experience and developments.* Annex 22. IEA. HPP-AN22-1. Trondheim, Norway. October. 119-129.

McLinden, M. O. and R. Radermacher. 1987. Methods for comparing the performance of pure and mixed refrigerants in the vapour compression cycle. *International Journal of Refrigeration.* Vol. 10 No.11. pp. 318-325.

Moffat, R. 1988. Describing the uncertainties in experimental results. *Experimental Thermal and Fluid Science.* Vol. 1. pp. 3-17.

Mulroy, W., M. Kauffeld, M. McLinden, and D. A. Didion. 1988, Experimental Evaluation of Two Refrigerant Mixtures in a Breadboard Air Conditioner, Proceedings of the 2nd DOE/ORNL Heat Pump Conference, Washington, D.C.

NIST. 1996. *NIST thermodynamic properties of refrigerants and refrigerant mixtures database.* (REFPROP 5.16). Gaithersburg, MD. USA

Pannock, J. and D. A. Didion. 1991. The performance of chlorine-free binary zeotropic refrigerant mixtures in a heat pump. NISTIR 4748. National Institute of Standards and Technology. Gaithersburg, MD. USA.

Rodecker, H. 1995. Propane, an alternative coolant for heat pumps?. *Compression systems with natural working fluids: applications, experience and developments.* Annex 22. IEA. HPP-AN22-1. Trondheim, Norway. October. 145-159.

Rothfleisch, P. I. and D. A. Didion. 1991.A performance evaluation of a variable speed, mixed refrigerant heat pump. NISTIR 5321. National Institute of Standards and Technology. Gaithersburg, MD. USA.

Rothfleisch, P. I. and D. A. Didion. 1993. A study of heat pump performance using mixtures of R32/R134a and R32/R125/R134a as 'drop in' working fluids for R22 with and without a liquid-suction heat exchanger. NISTIR 5321. National Institute of Standards and Technology. Gaithersburg, MD. USA.

Stene, Jorn. 1996. IEA Annex 22 - Compression systems with natural working fluids status and outlook for the project. *Applications for natural refrigerants.* Refrigeration Science and Technology Proceedings. International Institute of Refrigeration. Commissions B1, B2, E1, and E2. Aarhus, Sweden. September 3-6.

Treadwell, D. W. 1994. Application of propane (R-290) to a single packaged unitary air-conditioning product. ARI flammability workshop, Air-Conditioning and Refrigeration Institute. Arlington, VA.

Van Gerwen, R. J. M. and M. Verwoerd. 1997. Quantification and evaluation of safety risks related to the use of ammonia and hydrocarbons as refrigerants. *Compression systems with natural working fluids.* Annex 22. HPP-AN22-3. Gatlinburg, Tennessee, USA. October. 63-70.

Appendix A. Uncertainty Analysis

A. 1 General Remarks

The uncertainty analysis was performed to gain knowledge about the uncertainty of the measured and calculated data. This Appendix presents the major equations used for the uncertainty analysis.

A. 2 Theory

The uncertainty of a quantity R calculated from n independent measurements x_i is a function of the individual uncertainty of each measurement.

$$R = f(x_1, x_2, x_3, \ldots\ldots, x_n) \tag{A.1}$$

When each measurement, x_i, has a given uncertainty, dx_i, the maximum uncertainty of R is given by:

$$E_R = \left|\frac{\partial f}{\partial x_1} dx_1\right| + \left|\frac{\partial f}{\partial x_2} dx_2\right| + \left|\frac{\partial f}{\partial x_3} dx_3\right| + \ldots\ldots + \left|\frac{\partial f}{\partial x_n} dx_n\right|. \tag{A.2}$$

However, using the maximum error to judge the uncertainty of a calculated quantity is not common. Usually the standard deviation (root sum square) is regarded to be a much better approach to a quantity's uncertainty.

$$E_R = \sqrt{\left(\frac{\partial f}{\partial x_1} dx_1\right)^2 + \left(\frac{\partial f}{\partial x_2} dx_2\right)^2 + \left(\frac{\partial f}{\partial x_3} dx_3\right)^2 + \ldots\ldots + \left(\frac{\partial f}{\partial x_n} dx_n\right)^2} \tag{A.3}$$

The absolute error calculated with equation (A.3) is often converted to a relative error having the units of percent.

$$e_R = \frac{E_R}{R} 100 \tag{A.4}$$

A. 3 Temperature Measurements

Most of the temperature measurements performed for these tests were determined by thermocouples. Their voltage signals were measured with the data acquisition system and then converted into a temperature.

The equation used in the test rig's control program to convert the voltage signals into temperatures was a sixth degree polynomial of the form:

$$\vartheta = f(V) = \frac{9}{5}(A + B\,V + C\,V^2 + D\,V^3 + E\,V^4 + F\,V^5 + G\,V^6) + 32 \qquad \text{(A.5)}$$

where:

ϑ	=	temperature (°F)
V	=	measured voltage (μV)

If one premises that the uncertainty of the equation itself can be neglected, only one derivation is needed to evaluate the uncertainty in the temperature measurements.

$$\frac{\partial \vartheta}{\partial V} = \frac{9}{5}\left(B + 2C\,V + 3D\,V^2 + 4E\,V^3 + 5F\,V^4 + 6G\,V^5\right) \qquad \text{(A.6)}$$

According to the manufacturer of the datalogger voltmeter, the 95 % uncertainty of the voltage measurement (*VM*) was: $E_{VM} = dV(VM) = \pm\ 0.007\ \%\ of\ reading + 5\ \mu V$.

The measurement of a temperature (ϑ) actually is the measurement of the difference to a reference temperature. The data acquisition system provided a temperature compensation to 0 °C (32 °F) with a given uncertainty of: $E_{TC} = dTC = \pm 0.2236$ °C $= \pm 0.4025$ °F.

Rewriting equation A.3 for the measurement of the absolute temperature gives:

$$\vartheta = f(V) \qquad \text{(A.7)}$$

$$E_T = \sqrt{\left(\frac{\partial \vartheta}{\partial V}\,dVM\right)^2 + (dTC)^2} \qquad \text{(A.8)}$$

In addition to the common thermocouple measurements, the dew-point temperature in the air duct was measured to evaluate the humidity ratio of the moist air in the duct.

The manufacturer of the dew-point hygrometer specified the 95 % uncertainty in this measurement to be: $E_{T_{dew}} = dT_{dew} = \pm\ 0.05\ \%\ of\ reading$.

A. 4 Temperature Difference Measurements

The evaluation of the uncertainty of a temperature difference ($\Delta\vartheta$) measurement using a thermopile is slightly more complicated than that for a normal temperature measurement. The uncertainty evaluation is presented using the air duct temperature difference as an example, because this shows the most complicated case.

Again there are two independent uncertainties being part of the measurement uncertainty.

The first is the uncertainty caused by the voltage signal measurement, discussed in section A.3.
The cause for the second uncertainty influencing the measurement of a temperature difference is the nonlinear character of the temperature/voltage function (see equation A.5). The nonlinearity requires temperature at one end of the thermopile used for the temperature difference measurement to be known.

The temperature difference across the indoor coil was calculated using both the voltage signals of the temperature difference measurement (ΔV) and the average voltage signal ($V_{av.}$) of the entering temperature measurement of the air duct. The equation used to do so was:

$$\Delta\vartheta = f(V_{av.} + \Delta V) - f(V_{av.}) \tag{A.9}$$

The entering temperature was measured using 25 thermocouples equally distributed over the air duct's cross section. The average of the 25 temperature signals was considered to be the entering temperature. For the uncertainty in this average entering temperature the average voltage measurement uncertainty $E_{VM,av.}$ of the 25 measurements was calculated.

$$E_{VM,av.} = dV_{av}(VM) = \sum_{x=1}^{25} \frac{dV_{av.}(VM_x)}{25} \tag{A.10}$$

All 25 thermocouples were connected to the same temperature compensation. This means the overall uncertainty of the air's average entering temperature voltage signal $V_{av.}$ was:

$$dV_{av.} = \sqrt{E_{VM,av.}{}^2 + E_{TC}{}^2} = \sqrt{\left(dV_{av.}(VM)\right)^2 + \left(dV_{av.}(TC)\right)^2} \tag{A.11}$$

To evaluate equation A.11 the uncertainty in the temperature compensation must be rewritten to have the unit of μV. Using equation A.5 one finds that an uncertainty of $E_{TC} = dTC = \pm 0.2236° C = \pm\ 0.4025\ ^{o}F$ in the temperature compensation to 0 °C (32 °F) is equivalent to a voltage signal uncertainty of $dV_{av.}(TC) = \pm\ 8.6264\ \mu V$. As already mentioned, the uncertainty of the voltage signal measurement was given from manufacturer data.

The nonlinearity of the voltage/temperature function (A.5) causes an uncertainty *dslope* in the temperature difference that depends on the uncertainty in the entering temperature voltage signal $V_{av.}$.

$$E_{slope} = dslope = \Big|\left(\vartheta\left(V_{av.} + dV\right) - \vartheta\left(V_{av.}\right)\right) - \left(\vartheta\left(V_{av.} + dV_{av.} + \Delta V\right) - \vartheta\left(V_{av.} + dV_{av.}\right)\right)\Big| \tag{A.12}$$

where:

$V_{av.}$	=	entering temperature voltage signal (μV)
$dV_{av.}$	=	uncertainty of the entering temperature voltage signal (μV)
ΔV	=	temperature difference voltage signal (μV)

Remembering that an additional uncertainty in the temperature difference is caused by the voltage measurement of the temperature difference voltage signal (ΔV), the uncertainty of the air duct temperature difference is given to be:

$$E_{\Delta\vartheta} = d\Delta\vartheta = \left[\left(\frac{\partial\vartheta}{\partial V}\, d\Delta V\right)^2 + dslope^2\right]^{1/2} \tag{A.13}$$

A. 4 Uncertainty of the Air Side Capacity

The air side capacity of the heat pump was evaluated using the equation:

$$\dot{Q}_C = \dot{Q}_S + \dot{Q}_L \tag{A.14}$$

where:

$\dot{Q}_S$	=	sensible capacity, kW (*Btu/h*)
$\dot{Q}_L$	=	latent capacity, kW (*Btu/h*)

The sensible capacity is the heat needed to cool or heat the moist air passing the heat pump's indoor coil. The latent capacity is the heat rejected by water vapor condensing on the air coil. Condensation does not occur in the heating mode.

The two different capacities were calculated separately and then added (A.14). Therefore the uncertainty of the air-side capacity can be written as:

$$E_{\dot{Q}_C} = \left[\left(\frac{\partial\dot{Q}_C}{\partial\dot{Q}_S}\, d\dot{Q}_S\right)^2 + \left(\frac{\partial\dot{Q}_C}{\partial\dot{Q}_L}\, d\dot{Q}_L\right)^2\right]^{1/2} = \left(d\dot{Q}_S{}^2 + d\dot{Q}_L{}^2\right)^{1/2} \tag{A.15}$$

The equations for both the sensible and latent capacities and their uncertainties are presented on the following pages.

A. 4. 1 Uncertainty of the Sensible Capacity

According to ASHRAE Standard 116-1993 the sensible capacity Q_S is given by:

$$\dot{Q}_S = 3600\ C_D\ A_n(0.24 + 0.444\ W_{av.})(\vartheta_l - \vartheta)_e\left[\frac{2\ g_C\ \Delta p_n\ \rho_{nact}}{144(1-\beta^2)}\right]^{1/2} \quad \text{(A.16)}$$

where:

C_D	=	nozzle discharge coefficient (0.986)
A_n	=	nozzle throat area, m^2 (ft^2)
$W_{av.}$	=	$(W_e + W_l)$ / 2 average humidity ratio, kg H_2O/ kg dry air ($lb\ H_2O/lb\ dry\ air$)
$\vartheta_l - \vartheta_e$	=	indoor coil air temperature rise, °C (^oF)
g_C	=	gravity constant (32.174 $ft \cdot lb_m / lb_f \cdot s^2$)
Δp_n	=	static pressure drop across nozzle, kPa ($psia$)
ρ_{nact}	=	density of the moist air, kg/m^3 (lb / ft^3)
144	=	unit conversion factor from in^2 to ft^2
β	=	area relation factor (0.250723)

The partial derivatives required for the uncertainty analysis of Q_S are:

$$\frac{\partial \dot{Q}_S}{\partial A_n} = 3600\ C_D\ (0.24 + 0.444\ W_{av.})(\vartheta_l - \vartheta_e)\left[\frac{2\ g_C\ \Delta p_n\ \rho_{nact}}{144(1-\beta^2)}\right]^{1/2} \quad \text{(A.17)}$$

$$\frac{\partial \dot{Q}_S}{\partial W_e} = 1800\ C_D\ A_n\ 0.444\ (\vartheta_l - \vartheta_e)\left[\frac{2\ g_C\ \Delta p_n\ \rho_{nact}}{144(1-\beta^2)}\right]^{1/2} \quad \text{(A.18)}$$

$$\frac{\partial \dot{Q}_S}{\partial W_l} = 1800\ C_D\ A_n\ 0.444(\vartheta_l - \vartheta_e)\left[\frac{2\ g_C\ \Delta p_n\ \rho_{nact}}{144(1-\beta^2)}\right]^{1/2} \quad \text{(A.19)}$$

$$\frac{\partial \dot{Q}_S}{\partial(\vartheta_l - \vartheta_e)} = 3600\ C_D\ A_n(0.24 + 0.444\ W_{av.})\left[\frac{2\ g_C\ \Delta p_n\ \rho_{nact}}{144(1-\beta^2)}\right]^{1/2} \quad \text{(A.20)}$$

$$\frac{\partial \dot{Q}_S}{\partial \Delta p_n} = 1800\ C_D\ A_n(0.24 + 0.444\ W_{av.})(\vartheta_l - \vartheta_e)\left[\frac{2\ g_C\ \rho_{nact}}{144(1-\beta^2)\Delta p_n}\right]^{1/2} \quad \text{(A.21)}$$

$$\frac{\partial \dot{Q}_S}{\partial \rho_{nact}} = 1800\ C_D\ A_n(0.24 + 0.444\ W_{av.})(\vartheta_l - \vartheta_e)\left[\frac{2\ g_C\ \Delta p_n}{144(1-\beta^2)\rho_{nact}}\right]^{1/2} \quad \text{(A.22)}$$

$$\frac{\partial \dot{Q}_S}{\partial \beta} = 3600\ C_D\ A_n(0.24 + 0.444\ W_{av.})(\vartheta_1 - \vartheta_e)\beta\left[\frac{2\ g_C\ \Delta p_n\ \rho_{nact}}{144\ (1-\beta^2)^3}\right]^{1/2} \tag{A.23}$$

Using the above partial derivatives for rewriting equation A.3 gives:

$$E_{\dot{Q}_S} = \left[\left(\frac{\partial \dot{Q}_S}{\partial A_n}\ dA_n\right)^2 + \left(\frac{\partial \dot{Q}_S}{\partial W_e}\ dW_e\right)^2 + \left(\frac{\partial \dot{Q}_S}{\partial W_1}\ dW_1\right)^2 + \left(\frac{\partial \dot{Q}_S}{\partial \Delta p_n}\ d\Delta p_n\right)^2 + \right.$$
$$\left. + \left(\frac{\partial \dot{Q}_S}{\partial(\vartheta_1 - \vartheta_e)}\ d(\vartheta_1 - \vartheta_e)\right)^2 + \left(\frac{\partial \dot{Q}_S}{\partial \rho_{nact}}\ d\rho_{nact}\right)^2 + \left(\frac{\partial \dot{Q}_S}{\partial \beta}\ d\beta\right)\right]^{1/2} \tag{A.24}$$

Equation A.24 can be evaluated to give the uncertainty of $\dot{Q}_S$ if each of the individual uncertainties is known. However, A, β, W_e, W_1 and ρ_{nact} are calculated quantities, so their uncertainties were not known, but had to be calculated using equation A.3.

The flow in the air duct was measured using a venturi tube measurement. The nozzle throat area A_n, which is part of equation A.16, was calculated from the throat diameter. Thus its uncertainty can be evaluated very easily.

$$A_n = \frac{\pi\ d_n^{\,2}}{4} \tag{A.25}$$

$$E_{A_n} = \frac{\partial A_n}{\partial d_n}\ dd_n = \frac{\pi\ d_n}{2}\ dd_n \tag{A.26}$$

The uncertainty of the throat diameter was given to be: $E_{dn} = dd_n = \pm 0.254$ mm $= \pm$ 0.01 in.

The area ratio factor β was calculated using the equation:

$$\beta = \frac{A_n}{A_{en}} = \frac{d_n^{\,2}}{d_{en}^{\,2}} \tag{A.27}$$

Again, both areas were calculated using their diameter given by the manufacturer of the venturi tube. The partial derivatives used to evaluate the uncertainty in β were:

$$\frac{\partial \beta}{\partial d_n} = 2\ \frac{d_n}{d_{en}^{\,2}} \tag{A.28}$$

$$\frac{\partial \beta}{\partial d_{en}} = -2\,\frac{{d_n}^2}{{d_{en}}^3} \tag{A.29}$$

Using these derivatives to rewrite A.3 gives:

$$E_\beta = \left[\left(2\left({d_n}/{{d_{en}}^2}\right)dd_n\right)^2 + \left(-2\left({d_n}^2/{{d_{en}}^3}\right)dd_{en}\right)^2\right]^{1/2} \tag{A.30}$$

The required uncertainty in the inlet diameter was also
$E_{d_{en}} = dd_{en} = \pm 0.254$ mm $= \pm$ 0.01 in .

The humidity ratios W_e and W_l are a function of the water vapor pressure p_w and the atmospheric pressure p.

$$W = 0.62198 \cdot \frac{p_w}{p - p_w} \tag{A.31}$$

The factor 0.62198 comes from the ratio of the mole weights of the two components, water and air.

The required partial derivatives of equation A.31 are:

$$\frac{\partial W}{\partial p} = 0.62198\,\frac{p_w}{(p - p_w)^2} \tag{A.32}$$

$$\frac{\partial W}{\partial p_w} = 0.62198\,\frac{p}{(p - p_w)^2} \tag{A.33}$$

They lead to the uncertainty in W:

$$E_W = dW = \left[\left(\frac{\partial W}{\partial p}\,dp\right)^2 + \left(\frac{\partial W}{\partial p_w}\,dp_w\right)^2\right]^{1/2} \tag{A.34}$$

Unfortunately the water saturation pressure is a calculated quantity itself, which means its uncertainty had to be calculated.

The equation that was used to calculate the saturation pressure from the dew-point temperature, T_{dew}, (°R), is given below. The equation was assumed to cause no additional uncertainties.

$$p_w = EXP\left[\frac{C_8}{T_{dew}} + C_9 + C_{10}\ T_{dew} + C_{11}\ T_{dew}^{\ 2} + C_{12}\ T_{dew}^{\ 3} + C_{13}\ \ln T_{dew}\right] \tag{A.35}$$

The partial derivative of equation A.35 with respect to T_{dew} is:

$$\frac{\partial p_w}{\partial T_{dew}} = \left[\frac{-C_8}{T_{dew}^{\ 2}} + C_{10} + 2C_{11}\ T_{dew} + 3C_{12}\ T_{dew}^{\ 2} + \frac{C_{13}}{T_{dew}}\right] p_w \tag{A.36}$$

The uncertainty in p_W is now given by:

$$E_{p_w} = dp_w = \frac{\partial p_w}{\partial T_{dew}}\, dT_{dew} \tag{A.37}$$

As already mentioned in section A.3, the uncertainty of the dew-point temperature measurement was given to be: $E_{T_{dew}} = dT_{dew} = \pm\ 0.05\ \%$ of reading .

Finally, the uncertainty in the moist air's density ρ_{nact} had to be evaluated. The density was calculated using the ideal gas equation and the humidity ratio.

$$\rho_{nact} = \frac{p_n\ 144\ (1+W)}{R_a\ T_n\ (1+1.6078\ W)} \tag{A.38}$$

The factor 1.6078 is the ratio of the molar weights of air and water.

The partial derivatives of the A.38 are:

$$\frac{\partial \rho_{nact}}{\partial p_n} = \frac{144\ (1+W)}{R\ T_n\ (1+1.6078\ W)} \tag{A.39}$$

$$\frac{\partial \rho_{nact}}{\partial T_n} = \frac{-p_n\ 144\ (1+W)}{R\ T_n^{\ 2}\ (1+1.6078\ W)} \tag{A.40}$$

$$\frac{\partial \rho_{nact}}{\partial W} = \frac{-0.6078\ p_n\ 144}{R\ T_n\ (1+1.6078\ W)^2} \tag{A.41}$$

Rewriting equation A.3 with the above partial derivatives gives:

$$E_{\rho_{nact}} = \left[\left(\frac{\partial \rho_{nact}}{\partial p_n}\, dp_n\right)^2 + \left(\frac{\partial \rho_{nact}}{\partial T_n}\, dT_n\right)^2 + \left(\frac{\partial \rho_{nact}}{\partial W}\, dW\right)^2\right] \tag{A.42}$$

The pressure p_n in the nozzle throat was calculated as the difference of atmospheric pressure and nozzle pressure drop. The uncertainty of the nozzle pressure can be derived as follows:

$$p_n = p_{atm} - \Delta p \tag{A.43}$$

$$E_{p_n} = dp_n = \left[(dp_{atm})^2 + (d\Delta p)^2\right]^{1/2} \tag{A.44}$$

The uncertainties of the pressure measurements were given from manufacturer data:
$E_{p_{atm}} = dp_{atm} = \pm 0.3429 \text{ mm Hg} = \pm 0.0135 \text{ in Hg}$ and
$E_{Dp_n} = dDp_n = \pm 2.489 \text{ mm } H_2O = \pm 0.098 \text{ in } H_2O$.

A. 4. 2 Uncertainty of the Latent Capacity

The latent cooling capacity (ASHRAE Standard 116-1983) is given by:

$$\dot{Q}_L = 63600\ 60\ C_D\ A_n\ (W_e - W_l)\left[\frac{2\ g_C\ \Delta p_n\ \rho_{nact}}{144(1-\beta^2)}\right]^{1/2} \tag{A.44}$$

where:

C_D	=	nozzle discharge coefficient (0.986)
A_n	=	nozzle throat area (ft^2)
W_e	=	entering humidity ratio (lb H_2O/lb dry air)
W_l	=	leaving humidity ratio (lb H_2O/lb dry air)
g_C	=	gravity constant (32.174 $ft \cdot lb_m / lb_f \cdot s^2$)
Δp_n	=	static pressure drop across nozzle (psia)
ρ_{nact}	=	density of the moist air (lb / ft^3)
144	=	unit conversion factor from in^2 to ft^2
β	=	area relation factor (0.250723)

The partial derivatives of this equation are:

$$\frac{\partial \dot{Q}_L}{\partial A_n} = 63600\ 60\ C_D\ (W_e - W)_l\left[\frac{2\ g_C\ \Delta p_n\ \rho_{nact}}{144\ (1-\beta^2)}\right]^{1/2} \tag{A.45}$$

$$\frac{\partial \dot{Q}_L}{\partial W_e} = 63600\ 60\ C_D\ A_n\left[\frac{2\ g_C\ \Delta p_n\ \rho_{nact}}{144(1-\beta^2)}\right]^{1/2} \tag{A.46}$$

$$\frac{\partial \dot{Q}_L}{\partial W_l} = -63600\ 60\ C_D\ A_n \left[\frac{2\ g_C\ \Delta p_n\ \rho_{nact}}{144(1-\beta^2)} \right]^{1/2} \tag{A.47}$$

$$\frac{\partial \dot{Q}_L}{\partial \Delta p_n} = 31800\ 60\ C_D\ A_n\ (W_e - W_l) \left[\frac{2\ g_C\ \rho_{nact}}{144(1-\beta^2)\Delta p_n} \right]^{1/2} \tag{A.48}$$

$$\frac{\partial \dot{Q}_L}{\partial \rho_{nact}} = 31800\ 60\ C_D\ A_n\ (W_e - W)_l \left[\frac{2\ g_C\ \Delta p_n}{144(1-\beta^2)\rho_{nact}} \right]^{1/2} \tag{A.49}$$

$$\frac{\partial \dot{Q}_L}{\partial \beta} = 63600\ 60\ C_D\ A_n\ (W_e - W_l)\beta \left[\frac{2\ g_C\ \Delta p_n\ \rho_{nact}}{144(1-\beta^2)^3} \right]^{1/2} \tag{A.50}$$

If the above derivatives are used to rewrite equation A.3, one obtains the uncertainty of the latent capacity:

$$E_{\dot{Q}_L} = \left[\left(\frac{\partial \dot{Q}_L}{\partial A_n} dA_n \right)^2 + \left(\frac{\partial \dot{Q}_L}{\partial W_e} dW_e \right)^2 + \left(\frac{\partial \dot{Q}_L}{\partial W_l} dW_l \right)^2 + \right.$$
$$\left. + \left(\frac{\partial \dot{Q}_L}{\partial \Delta p_n} d\Delta p_n \right)^2 + \left(\frac{\partial \dot{Q}_L}{\partial \rho_{nact}} d\rho_{nact} \right)^2 + \left(\frac{\partial \dot{Q}_L}{\partial \beta} d\beta \right)^2 \right]^{1/2} \tag{A.51}$$

In this equation, all the needed uncertainties are known. Either because the quantities are directly measured or their uncertainties have already been calculated in Appendix A.4.1.

The final step was calculating the uncertainty of the air side capacity by using the now known uncertainties of sensible and latent capacity in equation A.15.

A. 5 Uncertainty of the COP

To calculate the COP's uncertainty it is necessary to know the uncertainties of the air-side capacity, $\dot{Q}$, and the mechanical power, P.

$$COP = \frac{\dot{Q}}{P} \tag{A.52}$$

The uncertainty of the COP is determined by:

$$E_{COP} = \left[\left(\frac{\partial COP}{\partial \dot{Q}} \, d\dot{Q} \right)^2 + \left(\frac{\partial COP}{\partial P} \, dP \right)^2 \right]^{1/2} = \left[\left(\frac{d\dot{Q}}{P} \right)^2 + \left(-\frac{\dot{Q}}{P^2} \, dP \right)^2 \right]^{1/2} \quad \text{(A.53)}$$

While the capacity's uncertainty is known from the previous equations, the uncertainty in the required mechanical work, which consists of the compressor power P_C and the HTF pumping power P_P, has not yet been evaluated.

The compressor power, P_C (lbf · ft / s), was calculated from measured values using the equation:

$$P_C = \frac{n}{30} \cdot \pi \cdot (Tor / 12) \quad \text{(A.54)}$$

where:

n	=	compressor speed (RPM)
Tor	=	compressor torque ($lb \cdot in$)
12	=	unit conversion factor from in to ft

The uncertainty in P_C is given by:

$$E_{W_C} = dP_C = \left[\left(\frac{\partial P_C}{\partial n} \, dn \right)^2 + \left(\frac{\partial P_C}{\partial Tor} \, dTor \right)^2 \right]^{1/2}$$

$$= \left[\left(\frac{Tor \, \pi}{30 \, 12} \, dn \right)^2 + \left(\frac{n \, \pi}{30 \;\; 12} \, dTor \right)^2 \right]^{1/2} \quad \text{(A.55)}$$

The uncertainties in the torque and RPM measurements were given from manufacturer data: $E_n = dn = \pm 5$ RPM ; $E_{Tor} = dTor = \pm 1$ % of reading .

The HTF pumping power was assumed to be 13.6 W/gpm (ARI Standard 330-1993). The uncertainty in the flow measurements was given from manufacturer data to be $E_{FM} = dFM = \pm 1$ % of reading . The uncertainty of the flow rate through both indoor and outdoor loops therefore is:

$$E_{\dot{V}_{HTF}} = d\dot{V}_{HTF} = \left[\left(\dot{V}_{IL} \; 0.01 \right)^2 + \left(\dot{V}_{OL} \; 0.01 \right)^2 \right]^{1/2} \quad \text{(A.56)}$$

This leads to the uncertainty in the pumping power:

$$E_{W_P} = dP_P = 8 \; \dot{V}_{HTF} \; d\dot{V}_{HTF} \quad \text{(A.57)}$$

Using equations A.55 and A.57 leads to an expression for the uncertainty in the mechanical work ingested by the heat pump:

$$E_W = dP = \left| \left(dP_C\right)^2 + \left(dP_P\right)^2 \right|^{1/2} \tag{A.58}$$

With the uncertainty of the mechanical work now known, equation A.55 can be evaluated.

A. 6 Uncertainty Analysis Results for Selected Tests

The performance of the uncertainty analysis showed, that over 90 % of the uncertainty in the air-side capacity was due to the pressure difference measurement between nozzle throat and air duct. Table A.1 gives an example of the error associated with COP and air-side capacity for several tests.

Table A.1: Measurement uncertainty for typical tests

Filename		Value	95 % Confidence Limit on Mean
R229805	COP	5.0	3.9 %
	Capacity	6.78 kW (23120 Btu/h)	3.7 %
R0332290	COP	5.3	2.7 %
	Capacity	9.10 kW (31036 Btu/h)	2.4 %
R2906001	COP	6.5	15.3 %
	Capacity	3.11 kW (10619 Btu/h)	15.2 %
H2906003	COP	4.4	14.1 %
	Capacity	2.71 kW (9261 Btu/h)	14.0 %